Microchim Acta (2017) 184:2739–2748
DOI 10.1007/s00604-017-2269-1

ORIGINAL PAPER

Binary nanocomposite based on Co_3O_4 nanocubes and multiwalled carbon nanotubes as an ultrasensitive platform for amperometric determination of dopamine

Arshid Numan[1] · Muhammad Mehmood Shahid[2] · Fatin Saiha Omar[1] · Saqib Rafique[2] · Shahid Bashir[3] · K. Ramesh[1] · S. Ramesh[1]

Received: 29 November 2016 / Accepted: 13 April 2017 / Published online: 3 May 2017

Abstract Composites containing cobalt oxide (Co_3O_4) nanocubes integrated with multiwall carbon nanotubes (MWCNT) were synthesized by a hydrothermal route. The fractions of MWCNTs in the composite were varied from 4, 8, 12, 16 and 20 wt.%, and the resulting materials are denoted as C1, C2, C3, C4 and C5, respectively. The formation of products with high structural crystallinity was confirmed by X-ray photoelectron spectroscopy, Raman spectroscopy and X-ray diffraction. A morphological study by field emission scanning electron microscopy and high resolution transmission electron microscopy showed the successful integration of Co_3O_4 nanocubes to the MWCNTs with an average particle size of ~32 nm. The surface of a glassy carbon electrode (GCE) was modified with the nanocomposites in order to evaluate the electrochemical performance of the nanocomposites. Cyclic voltammetry showed that the C4-modified GCE displays best performance in terms of oxidation potential and peak current in comparison to that of a bare GCE, Co_3O_4 nanocubes, or GCEs modified with C1, C2, C3 or C5. The detection limit (at an S/N ratio of 3) is 0.176 nM by using chronoamperometry, and the linear range is between 1 and 20 μM.

Keywords Electrochemical sensing · Amperometric detection · XPS · Urine analysis · HRTEM · Neurotransmitter · Electrocatalysis · XRD · FESEM · Raman spectroscopy

Electronic supplementary material The online version of this article (doi:10.1007/s00604-017-2269-1) contains supplementary material, which is available to authorized users.

✉ Arshid Numan
numan.arshed@yahoo.com

✉ S. Ramesh
rameshtsubra@gmail.com

[1] Centre for Ionics University of Malaya, Department of Physics, Faculty of Science, University of Malaya, 50603 Kuala Lumpur, Malaysia

[2] Department of Physics, Faculty of Science, University of Malaya, 50603 Kuala Lumpur, Malaysia

[3] Department of Chemistry, Faculty of Science, University of Malaya, 50603 Kuala Lumpur, Malaysia

Introduction

Dopamine is a key neurotransmitter that is present in the mammalian central nervous system and participates significantly in the activity of the hormonal, renal, cardiovascular and central nervous systems. It is responsible for communication of electrical signals between substantia nigra and various brain tissues. Additionally, it also helps to control hormonal balance and emotions. However, the abnormality in dopaminergic neurotransmission system results in various neurological diseases like schizophrenia, [1], Parkinson's disease [2], human immunodeficiency virus (HIV) infection [3] and Huntington's disease [4]. Consequently, quantitative determination of DA is very important. But various physiological biomolecules coexist with DA in a very high concentration in a biological system. Therefore, quantitative determination with good selectivity of DA is extremely important for the diagnosis and pathological understanding of several neurological diseases. For ex-vivo determination of DA, several techniques have been developed that includes: mass spectrometry [5], flow injection chemiluminescence fluorescence [6], surface enhanced Raman scattering [7], chromatography [8] optical absorption spectrophotometry [9] and micro dialysis [10]. But these analytical techniques suffer from the limitations of expensive instrumentation, large sample volumes, time consuming analysis and use of non-green solvents. On the other hand,

electrochemical methods are considered to be the best owing to their superior advantages like low cost, facile operation, high sensitivity with good selectivity, rapid response, reliability and reproducibility [11]. Since DA is a highly electroactive biomolecule, so electrochemical techniques are highly preferred for its quantitative determination. The main obstruction in the sensitive detection of DA level is the coexisting interfering biomolecules like ascorbic acid (AA) and uric acid (UA) in very high concentrations in biological tissues. These molecules have similar oxidation potential like DA, which makes electrochemical detection of DA more challengeable. In addition to this, the oxidation products of these molecules adsorb on the active sites of electrode which results in electrode fouling [12]. Consequently, the reproducibility and reusability of electrode decreases. Traditional unmodified electrodes are incapable to tackle these problems, which results in a poor performance. However, the surface modification of GCE plays significant role in enhancement of the performance of electrode in terms of sensitivity and selectivity [13]. Several materials have been investigated, which include conducting polymer based nanocomposites [14], metal, metal oxide nanoparticles [15, 16] and carbon based nanostructures [17] for the chemical modification of electrode to enhance the performance of the electrodes.

Noble metal/transition metal oxide nanoparticles embarked new era in the field of catalysis. Noble metals including Au, Pt, Pd and Ag proved themselves as an excellent candidate for various electrochemical and catalytic applications due to their marvelous electronic and electrocatalytic properties [18]. But their high price and scarcity hinders in commercializing them in a broad scope of applications. Hence, transition metal oxide nanoparticles attracted great attention owing to their low cost, unique structures and morphologies, tunable dimension sizes and abundance in nature. In the family of various transition metal oxides, cobalt oxide (Co_3O_4) breathed new life in the field of nanomaterials as a promising catalyst [19]. It is a P-type semiconductor with spinal structure bearing both direct and indirect band gap. Moreover, Co_3O_4 crystal consists of unique structure having magnetic Co^{2+} and non-magnetic Co^{3+} occupying tetrahedral and octahedral sites respectively, in the crystal [20]. These polar sites of Co_3O_4 crystal can play vital role in the catalytic activity, especially facilitating rapid charge transfer kinetics on the surface of the electrode. The high aspect ratio, unique crystal structure together with diverse morphologies make it as an ideal candidate for electrocatalytic applications. Due to these distinct characteristics, unaided Co_3O_4 nanostructures have been reported for electrocatalytic applications [21]. But the hybridizing the Co_3O_4 nanoparticles with conducting polymers and carbon based materials can significantly enhance the performance by improving the effective electrochemical surface area and reducing the charge transfer resistance. Recent reports unveil the potential of Co_3O_4 nanostructures supported on carbon based materials for energy conversion [22], energy storage [23] and electrochemical sensing applications [24].

Among carbon based materials, MWCNTs are highly active for electrochemical activities by virtue of their unique electronic structure. Owing to unique hollow structure, high porosity, enhanced electrochemical surface area and ballistic conductivity, MWCNT can serve as an excellent platform and efficient electron promoter for metal oxide nanostructures, especially in electrochemical sensing applications [25–27]. MWCNTs have great potential for electrochemical applications [28, 29]. Hence, by integrating Co_3O_4 with MWCNT can produce a synergistic effect which will result in superior route for electrochemical sensing applications.

In view of the above facts, herein we reported Co_3O_4 nanocubes integrated with MWCNT as a sensing interface for electrochemical detection of DA. There is no report available in the literature on the study of MWCNT decorated with Co_3O_4 nanocubes for the electrochemical sensing of DA. A one step hydrothermal route is used for the synthesis of MWCNT─Co_3O_4 nanocomposite. Hydrothermal route was preferred by virtue of its simplicity and choice of tuning various synthesis parameters (pH, temperature, time and concentration of regents or precursors). The appropriate amount of powdered reagents together with solvent can be put in a Teflon-lined autoclave and heated from room to elevated temperature and pressure for a fixed time. The electrolyte thermodynamics allows us in predicting optimum reaction conditions. The MWCNT─Co_3O_4 nanocomposite modified glassy carbon electrode (GCE) was used to investigate the electrocatalytic performance of fabricated nanocomposite. The cyclic voltammetric (CV) and amperometric results revealed that the MWCNT─Co_3O_4 nanocomposite is highly electroactive towards the oxidation of DA, even in the presence of physiological interfering species. The fabricated nanocomposite demonstrated superior performance in terms of low detection limit, high sensitivity and selectivity during the oxidation of DA.

Experimental

Materials

MWCNT (Outer diameter 10–15 nm and length, 1 μm) were obtained from Beytube Germany. Uric acid (UA), ascorbic acid (AA), Glucose, DA, cobalt acetate tetra hydrate ($Co(CH_3COO)_2.4H_2O$), Urea (CH_4N_2O), KCl and $Fe(CN)_6^{4-/3-}$ of analytical grade were purchased from Sigma Aldrich (http://www.sigmaaldrich.com/malaysia.html). Concentrated sulphuric acid (H_2SO_4, 98%), hydrochloric acid (HCl, 35%) and ammonia solution (NH_3, 25%) were purchased from Merck (http://www.merck.com/index.html). Deionized (DI) water was used throughout the experiments to prepare the solutions.

Preparation of MWCNT—Co_3O_4 nanocomposite

MWCNT—Co_3O_4 nanocomposite were synthesized by single step hydrothermal reaction. Before synthesis, MWCNT were functionalized by acid treatment. Appropriate amount of MWCNT powder was added in a mixture of 3:1 sulphuric/nitric acid (V:V) and stirred using magnetic stirrer for one hour. After this, mixture was sonicated for 6 h at room temperature followed by washing with DI water until pH reached to 7. The treated MWCNT were dried overnight at 50 °C in a vacuum oven. The acid treatment of MWCNT was done in order to increase their dispersion in water by functionalizing them with electronegative functional groups and removal of amorphous carbon as well as metal residue [30]. Later, 1 mM of Co $(CH_3COO)_2 4H_2O$ was dissolved in 45 mL DI water. Then, 15 mL of ammonia (6%) was added dropwise with a rate of 1 $mLmin^{-1}$ in above solution and the mixture was kept under vigorous stirring for one hour. At last, a solution containing MWCNT (4 wt.% (10 mg) in 15 mL) was added under bath sonication for 15 min and the resultant mixture was sealed in a stainless steel autoclave followed by hydrothermal reaction for 5 h at 150 °C. Finally, the precipitate of MWCNT—Co_3O_4 nanocomposite (designated as C1) was washed several times with deionized water and ethanol by centrifugation and dried at 60 °C in a hot air oven. Same experiments were repeated for the synthesis of Co_3O_4 nanocubes, C2, C3, C4 and C5 by using 0, 8 (20 mg), 12 (30 mg), 16 (40 mg), and 20 wt.% (50 mg) of MWCNT respectively.

Electrochemical measurements

Electrochemical measurements were carried out on multichannel Autolab (PGSTAT30) potentiostat workstation with conventional three electrode configuration. The MWCNT—Co_3O_4 nanocomposite modified GCE served as a working electrode, Ag/AgCl (3 M KCl) and platinum wire were used as reference and counter electrodes respectively. The electrochemical active surface area (ECSA) of all composites was calculated by running CVs of modified electrodes in 1 mM $Fe(CN)_6^{4-/3-}$ solution containing 0.1 M KCl at different scan rates (v) in standard three electrode cell system according to Randles-Sevcik eq. [31]. The surface of GCE was modified by dissolving catalyst powder in DI water (1 mg/ml) and drop coating 5 μL of the catalyst ink on the surface of GCE (diameter = 3 mm) which was subsequently dried at room temperature for one hour. Prior to every modification, GCE was cleaned electrochemically by potential cycling in 0.5 M H_2SO_4 using potential window between −1 to +1 V, followed by polishing with 1.0 μM and 0.3 μM alumina slurry. Phosphate buffer with neutral pH (7.2) was used as an electrolyte.

Preparation of real samples

In order to evaluate the performance of synthesized nanocomposite, analytical determination of DA in two urine samples was performed using the standard addition method. For this, two fresh urine samples from two healthy males were chosen as biological samples. The collected samples were filtered and stored at 4 °C immediately after collection. For further measurements, these samples were diluted 50 folds in 0.1 M Phosphate buffer (pH ~ 7.2).

Instrumentation

A JEOL JSM-7600F field emission scattering electron microscopy (FESEM) fitted with energy dispersive X-ray (EDX) and elemental mapping was employed to analyze the surface morphology and elemental mapping together with the EDX spectrum. High resolution transmission electron microscopy (HRTEM) micro images were taken by JEOL JEM-2100F in order to determine particle size distributions. Raman spectra were recorded using the Renishaw inVia 2000 system green laser emitting at 514 nm. The structural crystallinity of MWCNT—Co_3O_4 nanocomposite was studied using Philips X'pert X-ray diffractometer (XRD) with copper K_α radiation (λ = 1.5418 nm) at a scan rate of 0.02 degree per second. The surface chemistry and the composition of prepared composite was studied by X-ray photoelectron spectroscopy (XPS) analysis by using PHI 5000 Versa Probe Scanning ESCA Microprobe (PHI 5000 Versa Probe II, USA), fitted with monochromatic Al-Kα ($h\nu$ = 1486.6 eV) X-ray source.

Results and discussion

Surface morphology and microstructure analysis

HRTEM and FESEM micro images were taken to investigate microstructure and the surface morphology of the synthesized hybrid. Fig. 1 shows the HRTEM images of Co_3O_4 nanocubes, MWCNTs and MWCNT—Co_3O_4 nanocomposite. From Fig. 1a and b, sharp and well defined cubical structured Co_3O_4 nanoparticle with an average particle size of 32.5 nm are evident. Fig. 1a (inset) shows the distance between adjacent planes is 0.47 nm, corresponding to the inter-planar spacing of (111) plane of Co_3O_4 [32]. On the other hand, lose and unbundled acid treated MWCNT with broader length distributions are shown in Fig. 1c. The spread MWCNT were due to the electrostatic repulsion of electronegative functional groups on the surface of MWCNTs, which avoid them from bundling. During hydrothermal reaction, MWCNTs served as a platform for the growth of Co_3O_4 nanocubes. The functional groups on the cylindrical surface of MWCTNs served as nucleation sites for the growth. This resulted in uniform distribution of Co_3O_4

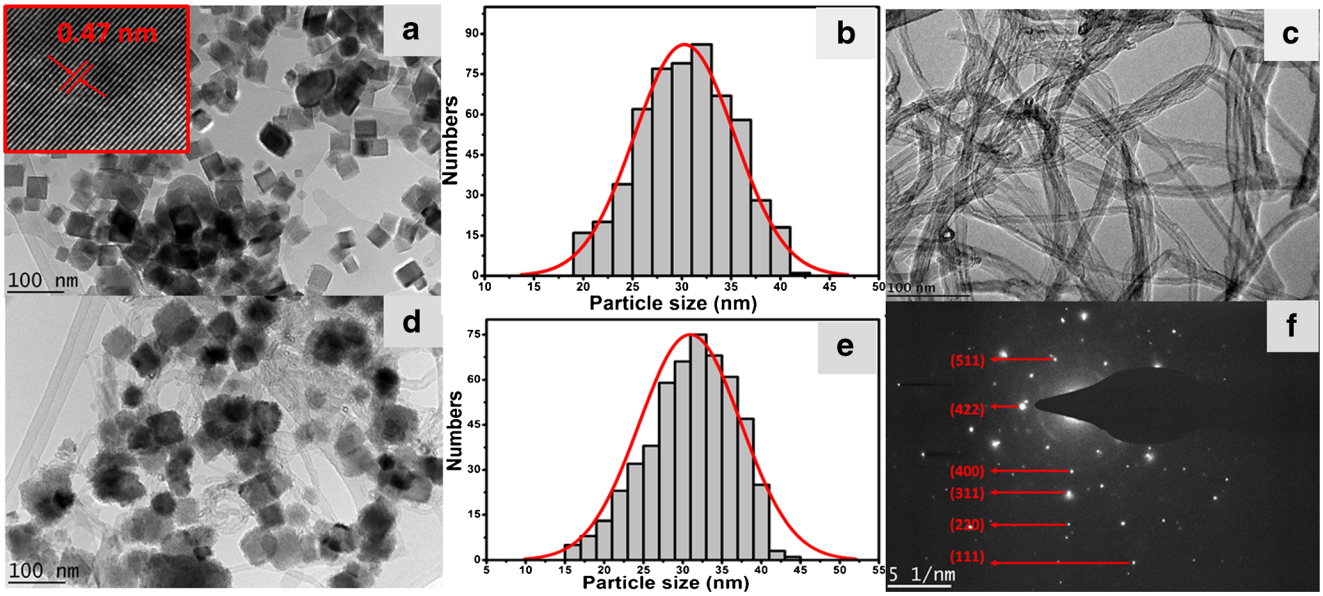

Fig. 1 HRTEM images of (**a**) MWCNT─Co_3O_4 nanocomposite (inset: lattice fringes), (**b**) particle size distribution of Co_3O_4 nanocubes (for total 500 particles), (**c**) acid treated MWCNT, (**d**) MWCNT─Co_3O_4 nanocomposite (C4), (**e**) particle size distribution of Co_3O_4 in composite MWCNT─Co_3O_4 and (**f**) SAED pattern of MWCNT─Co_3O_4 nanocomposite

nanocubes, which leads in the enhancement of electrochemical surface area (Fig. 1d). Moreover, the average particle size (32 nm) remained the same in the composite (Fig. 1e). The selected area electron diffraction (SAED) pattern of MWCNT─Co_3O_4 nanocomposite displayed six strong lattice fringes (2 2 0), (3 1 1), (4 0 0), (4 2 2), (5 1 1) and (4 4 0) correspond to the characteristic peaks of face centered cubic structured of Co_3O_4 demonstrated by XRD (Fig. S1b).

The surface morphology of synthesized nanocomposite was also confirmed by FESEM images (Fig. S2). Highly aggregated Co_3O_4 nanocubes were observed in Fig. S2a, b in the absence of MWCNT. However, upon addition of MWCNT, these aggregations were significantly decreased resulting highly exposed and well decorated Co_3O_4 nanocubes, which is shown in Fig. S2c, d.

The elemental distribution and purity of MWCNT─Co_3O_4 nanocomposite was analyzed by EDX elemental mapping (Fig. S4). The EDX spectrum shown in Fig. S4a (inset) displays the prominent peaks of cobalt, oxygen, carbon and silicon (arose from the substrate) without showing impurity peak. Fig. S4a shows the FESEM image of nanocomposite used for EDX elemental mapping. The independent elemental Co, O and C distributions are shown in Fig. S4b, c, d respectively, which display a uniform distribution of all elements. High density of red (Fig. S4b) and blue (S4d) dots are evidence of increased amounts of Co and C in the MWCNT─Co_3O_4 nanocomposite. Moreover, the combined elemental distribution shown in Fig. S4e depicts the homogeneous distribution of all color dots indicating the uniform decoration of Co_3O_4 nanocubes on MWCNTs.

XPS analysis

XPS analysis was performed to investigate the chemical composition and binding states of MWCNT─Co_3O_4 nanocomposite (Fig. 2). All binding energies found through XPS spectra were calibrated first using the C1s photoelectron peak at 284.8 eV as the reference. The survey scan spectrum of MWCNT─Co_3O_4 nanocomposite shown in Fig. 2a displayed the sharp and well defined peaks at 284.6, 530.1 and 779.8 eV corresponding to the characteristic peaks of C 1 s, Co 2p and O 1 s respectively. The core level deconvoluted spectrum of C 1 s in Fig. 2b consist of four peaks having binding energies at 284.6, 285.4, 288.6 and 289.0 eV. The peaks at 284.6 and 285.4 eV correspond to the non-oxygenated sp^2 (C = C) and sp^3 (C C) hybridized carbon, while the peaks at 288.6 and 289.0 eV are attributed to the presence of carbon in carbonyls (HO-C = O) and carboxyl (HO-C = O) functional groups [33, 34]. Fig. 2c depicts the high resolution spectrum of Co, containing two major peaks of binding energies at 780.6 and 795.5 eV correspond to the $2p_{3/2}$ and $2p_{1/2}$ respectively. The gap between two peaks is about 15 eV with the peak intensity ratio ($2p_{3/2}$: $2p_{1/2}$) of 2:1, which are the typical characteristic of standard of Co_3O_4 spectrum [35]. In addition to this, weak shake-up satellite peak at 786.9 eV is observed which confirmed the existence of Co^{2+} in the composite [36]. The core level spectrum of O 1 s is resolved into four Gaussian peaks at 529.7, 530.1, 531.6 and 533.3 eV (Fig. 2d). The peak at 529.7 eV is ascribed to the lattice oxygen of Co_3O_4. The other three peaks at higher binding energy values of 530.1, 531.6 and 533.3 eV are associated to the oxygen in cobalt monoxide

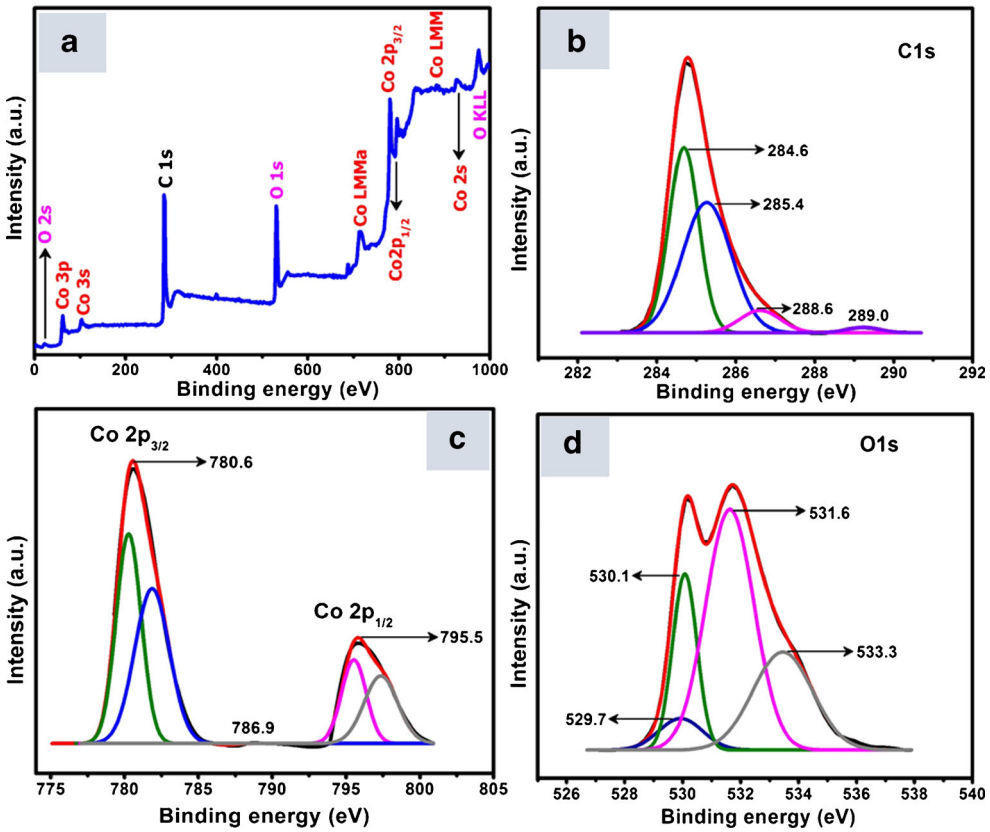

Fig. 2 **a** Survey spectrum of the MWCNT─Co_3O_4 nanocomposite (C4), **b** high resolution spectrum of the C 1 s region, **c** high resolution spectrum of the Co 2p region and **d** high-resolution spectrum of the O 1 s region

hydroxide ions, oxygen containing bonds (C-O/C = O) and water contents adsorbed on the surface of Co_3O_4 [37, 38].

Electrocatalytic performance of MWCNT─Co_3O_4 nanocomposite

DA is highly electroactive in nature, so upon application of electric potential it easily gets oxidized to dopamine quinone (DAQ) by liberating electrons. A schematic illustration of the redox behavior of DA at the MWCNT─Co_3O_4 nanocomposite modified GCE is portrayed in Fig. 3a. During forward potential sweep, DA is oxidized to DAQ by releasing two electrons at modified electrode surface, while on reverse potential sweep DAQ is reduced back to DA. This exchange of electrons at modified electrode surface produce Faradic current. The charge transfer kinetics and electrocatalytic behavior of the sensors were examined by recording cyclic voltammograms (CV) responses in 0.1 M Phosphate buffer (pH ~ 7.2) at scan rate of 50 mVs^{-1} in the presence of 0.5 mM DA. Fig. 3b shows the CVs of GCE modified with synthesized nanocomposites. Well defined redox peaks with anodic (E_{ap}) and cathodic (E_{cp}) peak at 210 and 40 mV respectively, with peak difference (ΔE) of 170 mV were shown by GCE. But upon modification of GCE with Co_3O_4 nanocubes, the peak potentials shifted to lower values leading to decrease in ΔE (150 mV) with improved redox peak current.

This confirmed the good catalytic activity of Co_3O_4 modified GCE towards DA. However, C1 modified GCE displayed noticeable shift in peak potentials to the low potentials with substantial enhancement in the current. The shift in peak potentials to the lower values can be attributed to the introduction of MWCNT to Co_3O_4 nanocubes, which acted as highly conductive wires facilitating fast charge transfer kinetics. In addition, MWCNT efficiently reduced the particle aggregations leading to the increase in effective electrochemical surface area resulting in the improvement of redox peak currents. Further improvement in redox peak currents together with shift in peak potentials to the lower potential was observed for C2, C3 and C4 modified GCE. But in case of C5, redox peak currents decreased significantly without any shift in peak potentials.

It is obvious that MWCNT─Co_3O_4 nanocomposite exhibit enhanced catalytic activity towards the electroxidation of DA compared to bare GCE and unsupported Co_3O_4 nanocubes. This revealed that MWCNT in the composite MWCNT─Co_3O_4 played a vital role during electrocatalytic activity by providing conducting platform which accelerated charge transport kinematics. Improved electrocatalytic response was observed for C4 modified GCE in terms of oxidation current and peak potential. It exhibited 4.3 fold higher peak oxidation current with very small peak difference (ΔE ~ 37 mV) compared to bare GCE. However, in the absence of DA, C4 modified GCE

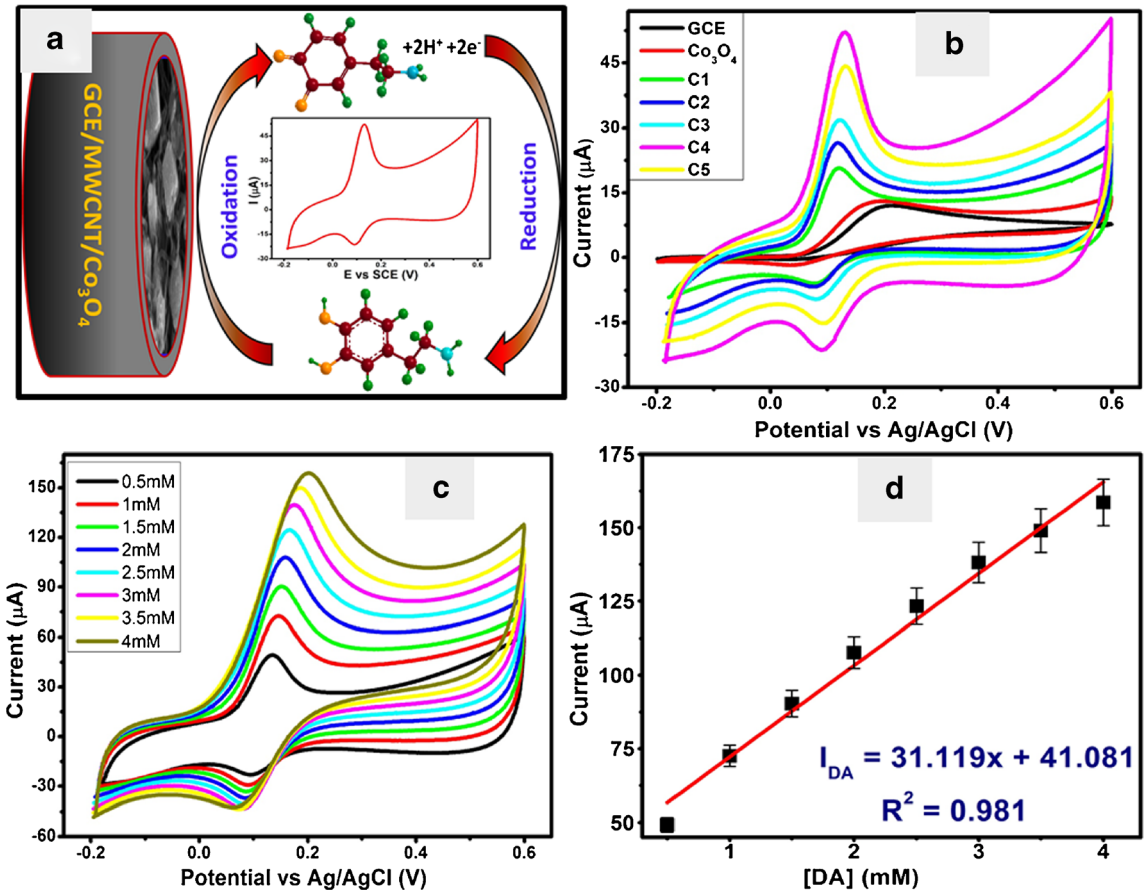

Fig. 3 **a** Schematic representation of electroxidation of DA at MWCNT─Co_3O_4 nanocomposite modified GCE. **b** CV curves for bare GCE, Co_3O_4 nanocubes, C1, C2, C3, C4 and C5 nanocomposite modified GCE for 0.5 mM DA in 0.1 M Phosphate buffer (pH ~ 7.2) at a scan rate of 50 $mV\,s^{-1}$, **c** CV curve of the rGO─Co_3O_4 nanocomposite modified GCE with the successive addition of different concentrations of DA, **d** Plot of anodic peak current vs molar concentration of DA

did not give any current response (Fig. S5). The poor electrocatalytic response of C1, C2 and C3 was due to the high aggregations of Co_3O_4 nanocubes, as the contents of MWCNT were insufficient for their uniform growth (Fig. S3a, b, c). Ultimately, the less faces of cubes were exposed to the electrolyte resulting decrease in the electrochemical surface area. However, less exposure of Co_3O_4 nanocubes in C5 due to higher contents of MWCNT which covered most of the cubes lead to the low catalytic response of C5 (Fig. S3d). The electrochemical surface measurement also revealed that C4 modified electrode possess enhanced electrochemical surface area (Table S1), which is in good agreement with current CV results. Thus, C4 was considered optimized composite for further studies.

The effect of scan rate on the electrocatalytic response of MWCNT─Co_3O_4 nanocomposite modified GCE towards DA oxidation was studied at different scan rate (from 10 to 225 mVs^{-1}) in 0.1 M Phosphate buffer (pH ~ 7.2) as background electrolyte (in the presence of 0.5 mM DA) using CV. Fig. S6a depicts well defined redox peaks, which were enhanced with increasing scan rate. Both anodic (I_{ap}) and cathodic (I_{cp}) peak currents were increased linearly with increase in slight shift in peak potentials. The calibration plot (Fig. S6b) of I_{ap} and I_{cp} with different scan rate showed a linear correlation (R^2 = 0.989 and 0.994), which confirmed that electron transfer reaction involved a surface-controlled process [39].

Fig. 3c shows the electrocatalytic responses of MWCNT─Co_3O_4 nanocomposite modified GCE at different molar concentrations of DA in 0.1 M of Phosphate buffer (pH ~ 7.2). Significantly, the oxidation peak current increased linearly with the addition of DA in the range of 0.5 to 5 mM and anodic peak potential underwent slightly positive shift (Fig. 3c). The plot of peak current (I_{pa}) and different of concentrations DA showed a linear plot with a slope value nearly equal to 1, which confirmed the electrochemical oxidation of DA follows the first order kinetics with respect to DA concentration at the C4 modified electrode (Fig. 3d).

Amperometric detection of DA at the MWCNT─Co_3O_4 nanocomposite modified GCE

The chrono-amperometric (CA) i-t curve technique is employed to detect the DA because it is a facile analytical

technique which facilitates low concentration detection of analytes and is convenient to perform interference studies. In order to investigate the sensing capability of all modified electrodes, each electrode was run at a fixed potential (applied potentials were the peak potentials from Fig. 3b) in homogeneously stirred 0.1 M Phosphate buffer (pH ~ 7.2) for the successive addition of 0.5 mM DA at a regular time interval of 60 s. Fig. 4a displays the amperometric responses of the bare GCE and GCE modified with Co_3O_4 nanocubes, C1, C2, C3, C4, and C5. It is obvious, from Fig. 4a that each electrode gave current response upon injection of 0.5 mM of DA. However, C4 modified GCE gave the highest current response which affirms the excellent oxidation capability of C4 towards DA. The enhanced electrocatalytic performance of C4 is attributed to the highly exposed Co_3O_4 nanocubes on MWCNT which lead in the augmentation of effective electrochemical surface area. These results are in good agreement to the aforementioned results discussed in section 4. Moreover, the calibration plots for the current response versus concentration values ranging from 0.5 to 5 mM showed linear relationship for all modified electrodes (Fig. 4b).

In order to calculate the limit of detection (LOD), repeated measurements were performed at low concentrations for C4 modified GCE. Fig. 4c depicts the amperometric response curve for MWCNT─Co_3O_4 nanocomposite (C4) modified GCE for the successive addition of DA with different concentrations in 0.1 M phosphate buffer (pH ~ 7.2) at an applied potential of +0.13 V. First, twenty spikes of 1 μM and then twenty spikes of 2 μM of DA were used to record the current. Upon each injection of DA with a sample interval of 60 s, C4 modified GCE gave significant current response. Fig. 4d shows the calibration plot of amperometric current response at different concentrations of DA. It is noticeable that calibration plot displayed two separate linear segments corresponding to the two different concentration ranges of DA. The first linear segment of calibration plot corresponds to the first concentration range of DA from 1 to 20 μM (20 injections with each injection of 1 μM) with a correlation coefficient of 0.992

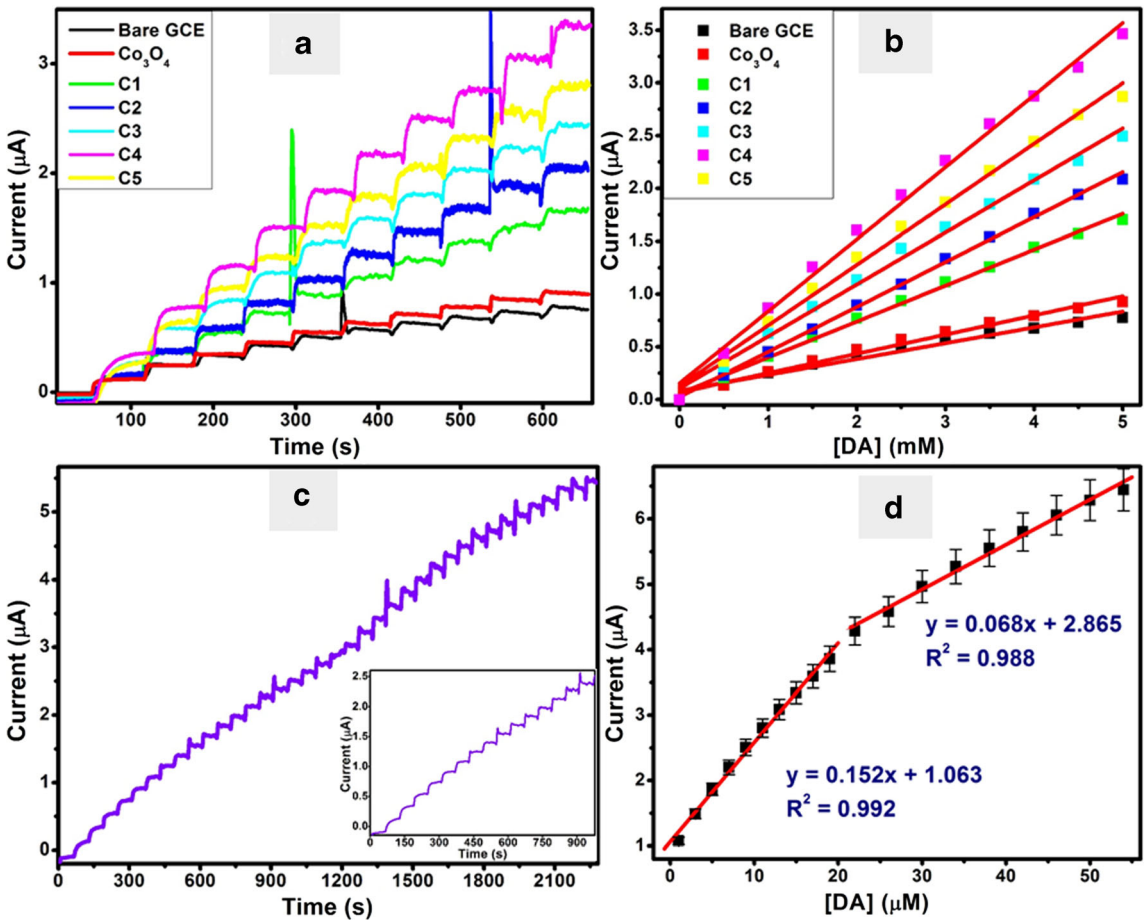

Fig. 4 **a** Amperometric i–t curves of bare GCE, Co_3O_4 nanocubes, C1, C2, C3, C4 and C5 modified GCE for the successive addition of 0.5 mM of DA in 0.1 M Phosphate buffer (pH ~ 7.2) at a regular interval of 60 s, (**b**) corresponding calibration plots of current versus concentration of DA. Applied potentials were the peak potentials from Fig. 4b, **c** Amperometric i–t curve of MWCNT─Co_3O_4 nanocomposite (C4) modified GCE for the successive addition of 1 mM DA in 0.1 M Phosphate buffer (pH 7.2) at an applied potential of +0.13 V with a regular interval of 60 s and (**d**) corresponding calibration plots of current versus concentration of DA

($n = 20$). The second linear segment is attributed to the second concentration range of DA from 20 to 60 (20 injections with each injection of 2 μM) with a correlation coefficient of 0.988 ($n = 20$). The current response was decreased even at higher concentrations of DA due to kinetic limitations of C4 modified electrode. Hence lower range was used to estimate the performance parameters for the sensor [40]. The LOD and limit of quantification (LOQ) were estimated to be 0.176 μM and 0.573 μM respectively, by using the standard deviation (SD) of the y-intercepts and the slope of the regression lines of lower range (S), (LOD = 3.3(SD/S) and LOQ = 10(SD/S)) [41]. The sensitivity of modified electrode is found to be 0.151 $\mu A \mu M^{-1}$. These results suggest that the fabricated MWCNT─Co_3O_4 nanocomposite sensor demonstrated enhance catalytic performance in terms of low LOD, wider linear range and good sensitivity towards DA detection. The comparison of the electrocatalytic performance of the MWCNT─Co_3O_4 nanocomposite modified GCE with some of the reported GCE based electrochemical sensors for the detection of DA is summarized in Table S2.

Interference studies

During electrochemical sensing of an analyte, it is important for the sensor to detect the target molecule selectively without producing any interfering current response. The ascorbic acid (AA) and uric acid (UA) are the two important interfering agents which coexist with DA. Therefore, it is very important to evaluate the detection capability of a DA sensor in the presence of AA and UA. The selectivity of the MWCNT─Co_3O_4 nanocomposite based sensor for the detection of DA was examined in the presence of different interferents like UA, AA, glucose, and urea by using CA. Usually, square wave voltammetry (SWV) and differential pules voltammetry (DPV) are employed to evaluate the selectivity of a DA in the presence of UA and AA. But in case of CA, the selectivity of DA can be evaluated even in the presence of higher number of potential interferents such as UA, AA, glucose, urea and NaCl etc. In addition to this, oxidation potential of DA is very close to AA and UA, so it is very difficult to get separate and well defined oxidation peaks for each analyte. However these problems are avoided in CA. Fig. 5 depicts the recorded amperometric i–t curve response for the consecutive additions of DA and interferents in a homogeneously stirred 0.1 M Phosphate buffer at a constant applied potential of +0.13 V. Three consecutive injections of DA (each of 0.5 mM) were used at the start and it was found that each injection gave significant current response. After this, UA, AA, glucose and urea were injected respectively, with the sample time of 60 s. However, no obvious increase in current response was observed for all interfering species except AA even at fifty fold higher concentration then DA.

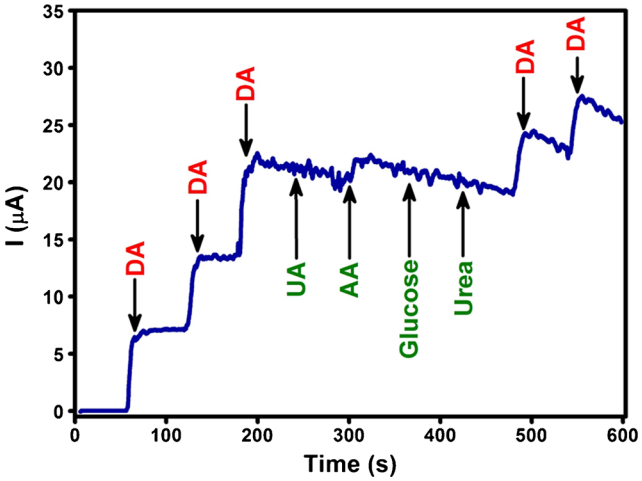

Fig. 5 Amperometric i–t curve of MWCNT─Co_3O_4 nanocomposite (C4) modified GCE for the successive addition of DA and interfering species each of 0.5 mM in 0.1 M PBS at a regular interval of 60 s. The applied potential was +0.13 V

Compared to DA, only 12% current response was observed for AA which indicates that the signal of DA is much stronger compared to AA. These results revealed that the sensor possesses good selectivity towards the quantitative determination of DA even in the presence of common physiological interferents.

Stability and reproducibility

In order to evaluate the performance and reliability of the sensor in real application, analytical determination of DA in two urine samples was performed using standard addition method. The analytical results were summarized in Table S3. To ascertain the accuracy of the results, different concentrations of DA were added in urine containing Phosphate buffer and detected. The recovery of spiked sample ranged between 99.1 to 104%, which is indication of the successful application of MWCNT─Co_3O_4 nanocomposite for the detection of DA.

For the stability study of the sensor, CV response of C1 modified GCE was recorded for DA in a range between −0.2 and 0.6 V at scan rate of 50 mV s^{-1}. The CV response was recorded on after every two days for two weeks. The peak current was considered as a factor for indicating the stability of the modified electrode. Here, I is the current response of fresh sensor and I_0 is the current response after storage as shown in Fig. S6. A 16.7% decrease in the anodic peak current with slight shift in peak potential was observed after two weeks. This revealed that C1 modified GCE can also withstand being stored in the solution for a period of time (two weeks) and the electrocatalytic performance remain almost unchanged, which confirms that modified electrode is very stable and reproducible for the detection of DA.

Additionally, operational stability of MWCNT─Co_3O_4 nanocomposite modified GCE was also evaluated by

performing CA in 0.1 M Phosphate buffer containing 0.5 mM DA at a constant potential of +0.13 V for 2500 s. A very stable current response was observed and only 7.32% decay in the current was observed after 2500 s (Fig. S7). This confirms the excellent operational stability of modified GCE.

Conclusions

MWCNT─Co_3O_4 nanocomposite was successfully synthesized by hydrothermal method for the electrochemical detection of DA. The composition, crystallinity and phase purity was confirmed by XPS, Raman spectroscopy and XRD. FESEM and HRTEM images were obtained to confirm the integration of Co_3O_4 nanocubes with MWCNT. For electrocatalytic performance towards DA oxidation, the surface of GCE was modified with the synthesized nanocomposites. The CV results demonstrate that C4 modified GCE exhibited enhanced electrocatalytic performance in terms of oxidation potential and peak current in comparison to its counterpart electrodes. The excellent catalytic activity was due to the less aggregations of Co_3O_4 nanocubes which resulted in a high electrochemical surface area. The interference studies showed that C4 demonstrates promising recognition towards the detection of DA in the presence of different types of physiological interfering species. However, for AA a slight response was observed during selectivity studies. In addition, sensor also displayed satisfactory results in real samples. The electrochemical sensing results suggest that MWCNT─Co_3O_4 nanocomposite endow excellent catalytic activity with high stability and reproducibility. It provides great potentials for the practical detection DA in urine and blood samples.

Acknowledgements This work was supported by the High Impact Research Grant (H-21001-F000046), Fundamental Research Grant Scheme (FP012-2015A) from Ministry of Education, Malaysia and Postgraduate Research Grant (PG119-2015A).

Compliance with ethical standards The author(s) declare that they have no competing interests.

References

1. Aurora R, Kristo D, Bista S, Rowley J (2012) Zak RS; Casey KR; Lamm CI; Tracy SL; Rosenberg RS. The treatment of restless legs syndrome and periodic limb movement disorder in adults—an update for 2012: practice parameters with an evidence-based systematic review and meta-analyses. Sleep 35(8):1039–1062
2. Obata T (2002) Dopamine efflux by MPTP and hydroxyl radical generation. J Neural Transm 109(9):1159–1180
3. Ensafi AA, Taei M, Khayamian T (2009) A differential pulse voltammetric method for simultaneous determination of ascorbic acid, dopamine, and uric acid using poly (3-(5-chloro-2-hydroxyphenylazo)-4, 5-dihydroxynaphthalene-2, 7-disulfonic acid) film modified glassy carbon electrode. J Electroanal Chem 633(1):212–220
4. Wightman RM, May LJ, Michael AC (1988) Detection of dopamine dynamics in the brain. Anal Chem 60(13):769A–793A
5. Holdiness MR, Rosen MT, Justice JB, Neill DB (1980) Gas chromatographic-mass spectrometric determination of dopamine in subregions of rat brain. J Chromatogr A 198(3):329–336
6. Deftereos NT, Calokerinos AC, Efstathiou CE (1993) Flow injection chemiluminometric determination of epinephrine, norepinephrine, dopamine and L-dopa. Analyst 118(6):627–632
7. Kaya M, Mr V (2012) New approach for the surface enhanced resonance Raman scattering (SERRS) detection of dopamine at picomolar (pM) levels in the presence of ascorbic acid. Anal Chem 84(18):7729–7735
8. Zhou Y, Yan H, Xie Q, Huang S, Liu J, Li Z, Ma M, Yao S (2013) Simultaneous analysis of dopamine and homovanillic acid by high-performance liquid chromatography with wall-jet/thin-layer electrochemical detection. Analyst 138(23):7246–7253
9. Mamiński M, Olejniczak M, Chudy M, Dybko A, Brzózka Z (2005) Spectrophotometric determination of dopamine in microliter scale using microfluidic system based on polymeric technology. Anal Chim Acta 540(1):153–157
10. Watson CJ, Venton BJ, Kennedy RT (2006) In vivo measurements of neurotransmitters by microdialysis sampling. Anal Chem 78(5): 1391–1399
11. Abdelwahab AA, Shim Y-B (2015) Simultaneous determination of ascorbic acid, dopamine, uric acid and folic acid based on activated graphene/MWCNT nanocomposite loaded au nanoclusters. Sensors Actuators B Chem 221:659–665
12. Omar FS, Duraisamy N, Ramesh K, Ramesh S (2016) Conducting polymer and its composite materials based electrochemical sensor for nicotinamide adenine dinucleotide (NADH). Biosens Bioelectron 79:763–775
13. Nazemi Z, Shams E, Amini MK (2010) Covalent modification of glassy carbon electrode by Nile blue: Preparation, electrochemistry and electrocatalysis. Electrochim Acta 55(24):7246–7253
14. Palanisamy S, Thangavelu K, Chen S-M, Gnanaprakasam P, Velusamy V, Liu X-H (2016) Preparation of chitosan grafted graphite composite for sensitive detection of dopamine in biological samples. Carbohydr Polym 151:401–407
15. Liu Y, She P, Gong J, Wu W, Xu S, Li J, Zhao K, Deng A (2015) A novel sensor based on electrodeposited au–Pt bimetallic nanoclusters decorated on graphene oxide (GO)–electrochemically reduced GO for sensitive detection of dopamine and uric acid. Sensors Actuators B Chem 221:1542–1553
16. Palanisamy S, Ku S, Chen S-M (2013) Dopamine sensor based on a glassy carbon electrode modified with a reduced graphene oxide and palladium nanoparticles composite. Microchim Acta 180(11–12): 1037–1042
17. Fernandes DM, Costa M, Pereira C, Bachiller-Baeza B, Rodríguez-Ramos I, Guerrero-Ruiz A, Freire C (2014) Novel electrochemical sensor based on N-doped carbon nanotubes and Fe 3 O 4 nanoparticles: simultaneous voltammetric determination of ascorbic acid, dopamine and uric acid. J Colloid Interface Sci 432:207–213
18. Pandikumar A, How GTS, See TP, Omar FS, Jayabal S, Kamali KZ, Yusoff N, Jamil A, Ramaraj R, John SA (2014) Graphene and its nanocomposite material based electrochemical sensor platform for dopamine. RSC Adv 4(108):63296–63323
19. Moro F, Tang SVY, Tuna F, Lester E (2013) Magnetic properties of cobalt oxide nanoparticles synthesised by a continuous hydrothermal method. J Magn Magn Mater 348:1–7
20. Xie X, Li Y, Liu Z-Q, Haruta M, Shen W (2009) Low-temperature oxidation of CO catalysed by Co3O4 nanorods. Nature 458(7239): 746–749
21. Mu J, Zhang L, Zhao M, Wang Y (2013) Co 3 O 4 nanoparticles as an efficient catalase mimic: properties, mechanism and its

electrocatalytic sensing application for hydrogen peroxide. J Mol Catal A Chem 378:30–37
22. Shahid MM, Pandikumar A, Golsheikh AM, Huang NM, Lim HN (2014) Enhanced electrocatalytic performance of cobalt oxide nanocubes incorporating reduced graphene oxide as a modified platinum electrode for methanol oxidation. RSC Adv 4(107): 62793–62801
23. Numan A, Duraisamy N, Omar FS, Mahipal Y, Ramesh K, Ramesh S (2016) Enhanced electrochemical performance of cobalt oxide nanocube intercalated reduced graphene oxide for supercapacitor application. RSC Adv 6(41):34894–34902
24. Numan A, Shahid MM, Omar FS, Ramesh K, Ramesh S (2017) Facile fabrication of cobalt oxide nanograin-decorated reduced graphene oxide composite as ultrasensitive platform for dopamine detection. Sensors Actuators B Chem 238:1043–1051
25. Bathinapatla A, Kanchi S, Singh P, Sabela MI, Bisetty K (2015) Fabrication of copper nanoparticles decorated multiwalled carbon nanotubes as a high performance electrochemical sensor for the detection of neotame. Biosens Bioelectron 67:200–207
26. Lu L-M, Zhang X-B, Shen G-L, Yu R-Q (2012) Seed-mediated synthesis of copper nanoparticles on carbon nanotubes and their application in nonenzymatic glucose biosensors. Anal Chim Acta 715:99–104
27. Sanghavi BJ, Wolfbeis OS, Hirsch T, Swami NS (2015) Nanomaterial-based electrochemical sensing of neurological drugs and neurotransmitters. Microchim Acta 182(1–2):1–41
28. Yang Y, Zhang H, Huang C, Jia N (2016) MWCNTs-PEI composites-based electrochemical sensor for sensitive detection of bisphenol a. Sensors Actuators B Chem 235:408–413
29. Qiu X, Lu L, Leng J, Yu Y, Wang W, Jiang M, Bai L (2016) An enhanced electrochemical platform based on graphene oxide and multi-walled carbon nanotubes nanocomposite for sensitive determination of sunset yellow and Tartrazine. Food Chem 190:889–895
30. Datsyuk V, Kalyva M, Papagelis K, Parthenios J, Tasis D, Siokou A, Kallitsis I, Galiotis C (2008) Chemical oxidation of multiwalled carbon nanotubes. Carbon 46(6):833–840t
31. Bard AJ, Faulkner LR, Leddy J, Zoski CG (1980) Electrochemical methods: fundamentals and applications, 2nd ed., John Wiley and Sons, New York
32. Panwar V, Al-Nafiey A, Addad A, Sieber B, Roussel P, Boukherroub R, Jain SL (2015) Magnetic co 3 O 4/reduced graphene oxide nanocomposite as a superior heterogeneous catalyst for one-pot oxidative esterification of aldehydes to methyl esters. RSC Adv 5(108):88567–88573
33. Abouali S, Akbari Garakani M, Zhang B, Xu Z-L, Kamali Heidari E, J-q H, Huang J, Kim J-K (2015) Electrospun carbon nanofibers with in situ encapsulated Co3O4 nanoparticles as electrodes for high-performance supercapacitors. ACS Appl Mater Interfaces 7(24):13503–13511
34. Tan Y, Gao Q, Li Z, Tian W, Qian W, Yang C, Zhang H (2016) Unique 1D Co_3O_4 crystallized nanofibers with (220) oriented facets as high-performance lithium ion battery anode material. Sci Rep 6: 26460. doi:10.1038/srep26460
35. Tan Y, Gao Q, Yang C, Yang K, Tian W, Zhu L (2015) One-dimensional porous nanofibers of Co_3O_4 on the carbon matrix from human hair with superior lithium ion storage performance. Sci Rep 55:12382. doi:10.1038/srep12382
36. Huang H, Zhu W, Tao X, Xia Y, Yu Z, Fang J, Gan Y, Zhang W (2012) Nanocrystal-constructed mesoporous single-crystalline Co3O4 nanobelts with superior rate capability for advanced lithium-ion batteries. ACS Appl Mater Interfaces 4(11):5974–5980
37. Xiong S, Chen JS, Lou XW, Zeng HC (2012) Mesoporous Co3O4 and CoO@ C Topotactically transformed from chrysanthemum-like CO (CO3) 0.5 (OH)· 0.11 H2O and their lithium-storage properties. Adv Funct Mater 22(4):861–871
38. Li B, Xie Y, Wu C, Li Z, Zhang J (2006) Selective synthesis of cobalt hydroxide carbonate 3D architectures and their thermal conversion to cobalt spinel 3D superstructures. Mater Chem Phys 99(2):479–486
39. Shahid MM, Rameshkumar P, Pandikumar A, Lim HN, Ng YH, Huang NM (2015) An electrochemical sensing platform based on a reduced graphene oxide–cobalt oxide nanocube@ platinum nanocomposite for nitric oxide detection. J Mater Chem A 3(27):14458–14468
40. How GTS, Pandikumar A, Ming HN, Ngee LH (2014) Highly exposed {001} facets of titanium dioxide modified with reduced graphene oxide for dopamine sensing. Scientific Reports 4:5044. doi:10.1038/srep05044. http://www.nature.com/articles/srep05044#supplementary-information
41. Jayabal S, Ramaraj R (2013) Synthesis of core/shell au/ag nanorods embedded in functionalized silicate sol–gel matrix and their applications in electrochemical sensors. Electrochim Acta 88:51–58